

Ground state magnetic structure of Mn_3Ge

J.-R. Soh,¹ F. de Juan,^{2,3} N. Qureshi,⁴ H. Jacobsen,¹ H.-Y. Wang,^{5,6} Y.-F. Guo,⁵ and A. T. Boothroyd^{1,*}

¹*Department of Physics, University of Oxford, Clarendon Laboratory, Parks Road, Oxford OX1 3PU, UK*

²*Donostia International Physics Center, 20018 Donostia-San Sebastian, Spain*

³*IKERBASQUE, Basque Foundation for Science, Maria Diaz de Haro 3, 48013 Bilbao, Spain*

⁴*Institut Laue-Langevin, 6 rue Jules Horowitz, 38042 Grenoble Cedex 9, France*

⁵*School of Physical Science and Technology, ShanghaiTech University, Shanghai 201210, China*

⁶*University of Chinese Academy of Sciences, Beijing 100049, China*

(Dated: April 30, 2020)

We have used spherical neutron polarimetry to investigate the magnetic structure of the Mn spins in the hexagonal semimetal Mn_3Ge , which exhibits a large intrinsic anomalous Hall effect. Our analysis of the polarimetric data finds a strong preference for a spin structure with E_{1g} symmetry relative to the D_{6h} point group. We show that weak ferromagnetism is an inevitable consequence of the symmetry of the observed magnetic structure, and that sixth order anisotropy is needed to select a unique ground state.

PACS numbers: 75.25.+z, 61.12.Ld

Recently, Mn_3Ge was found to display a large anomalous Hall effect (AHE) of $\sim 50 \Omega^{-1}\text{cm}^{-1}$ at room temperature [1, 2]. This finding was interesting because Mn_3Ge is an antiferromagnetic (AFM) metal, and a large AHE is usually restricted to ferromagnetic metals [3]. Moreover, the spontaneous AHE in Mn_3Ge is strongly anisotropic, and can be switched with a small applied magnetic field [1, 2]. From a technological standpoint, the concept of an AFM memory device that can be switched is very attractive as there is no demagnetization field, which limits the size of ferromagnetic materials. The prospect of scaling down the size of magnetic devices has prompted many studies of thin-film Mn_3Ge [4–9], and the initial results look promising.

Naturally, it is of interest to understand how such a large AHE can occur in an antiferromagnet, and there has been a spate of theoretical studies [2, 10–18]. The symmetries of non-collinear antiferromagnets generically do not forbid the AHE, and several of the recent studies have concluded that the particular chiral pattern of Mn spins can lead to large Berry curvature at the Fermi surface and thus a large AHE, as predicted by an earlier work [19]. The AHE has also attracted recent interest as a signature of Weyl points, which appear relatively near the Fermi level in this system. The theoretical work has led to predictions of other anomalous transport phenomena in Mn_3Ge , including the anomalous Nernst [10], spin Nernst [10] and spin Hall effects [2, 12, 17]. These theoretical predictions depend on the fine details of the magnetic structure, so it is important to work with an unambiguous solution for the zero-field magnetic order.

The hexagonal unit cell of Mn_3Ge can be described by the $P6_3/mmc$ space group (No. 194) with Mn and Ge on the $6h$ and $2c$ Wyckoff sites, respectively. In practice, a small excess of Mn is needed to stabilize the hexagonal phase, so that the true chemical formula is $\text{Mn}_{3+x}\text{Ge}_{1-x}$, with $x = 0.04$ to 0.09 for samples pre-

pared from the melt [20]. For simplicity, we shall continue to write the formula as Mn_3Ge . The Mn atoms are arranged in a Kagome pattern, with two Kagome layers per unit cell stacked along the c -axis with an in-plane displacement. Antiferromagnetic order of the Mn

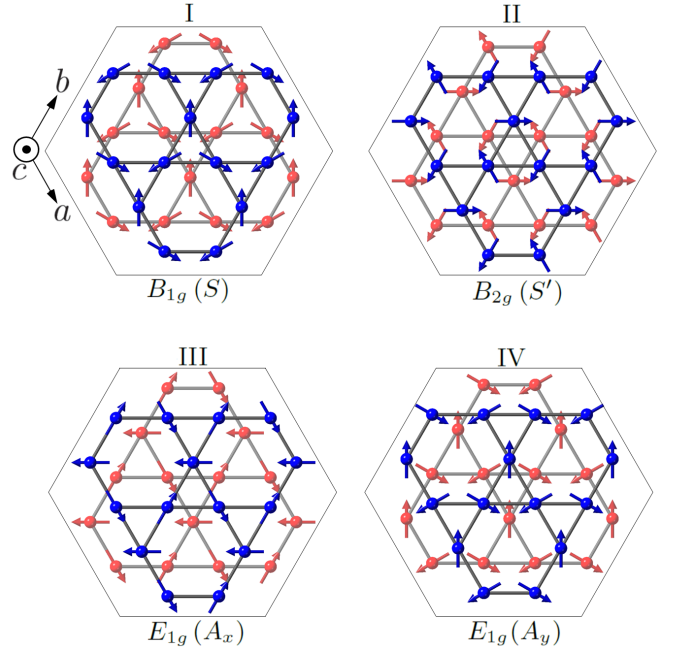


FIG. 1. Symmetry-allowed magnetic structures of the Mn spins in $\text{Mn}_3\text{Sn}/\text{Mn}_3\text{Ge}$, viewed in projection down the c axis. The red and blue arrows correspond to Mn at Wyckoff position $6h$ with $z = 1/4$ and $3/4$, respectively. Ge atoms are omitted for clarity. Only configurations in which the spins related by inversion symmetry are parallel and lie in the basal plane are considered. The structures shown transform according to the irreducible representations (irreps) of the D_{6h} point group. The symmetry label of the irreps is given, together with our labels for the order parameters (in parentheses).

spins sets in at $T_N \simeq 380$ K, and below roughly the same temperature weak ferromagnetism in the basal plane is observed in magnetisation measurements, with a zero-field remnant moment of about $0.006 \mu_B$ per Mn at low temperature [1, 2, 21, 22].

Initial neutron powder diffraction studies of Mn_3Ge in the magnetically-ordered phase revealed that the Mn spins lie in the ab plane in a 120° structure, with a $\mathbf{k} = \mathbf{0}$ magnetic propagation vector and an ordered moment of about $2.5 \mu_B$ [21, 23]. Experiments indicate that the transition to magnetic order in Mn_3Ge is second-order [1, 2], so based on Landau's theory of phase transitions we expect the magnetic structure of Mn_3Ge to be described by a single irreducible representation (irrep) of the D_{6h} point group. Symmetry analysis shows that there are four distinct $\mathbf{k} = \mathbf{0}$ structures with ab -plane spin alignment and 120° order (see Supplemental Material [22]). These are shown in Fig. 1. Which of these structures is correct, however, cannot be determined unambiguously from the unpolarized-neutron powder diffraction data. Subsequently, magnetic diffraction studies were performed on Mn_3Ge single crystals with polarized neutrons [24, 25]. However, the polarization of the scattered beam, which contains important information for a complete magnetic structure determination [26–29] was not analyzed in these experiments. Moreover, the half-polarized diffraction technique employed in these studies requires the sample to be in an applied field which preferentially orients the Mn moments along the field direction, undermining the elucidation of the true ground state magnetic structure.

To overcome these shortcomings, Brown *et al.* [30] used spherical neutron polarimetry (SNP) — a more sophisticated polarized neutron technique, which probes the sample in zero field (see below) — to study the magnetic structure of Mn_3Sn , which is isostructural to Mn_3Ge . They were able to constrain the spin structure of Mn_3Sn to be either model III or IV as shown in Fig. 1, but found that both gave an equally good fit to their data [30].

In this work, we used SNP to investigate the zero-field AFM structure of Mn_3Ge by a similar method to that of Brown *et al.* [30]. We show unambiguously that the magnetic structure of Mn_3Ge is described by model IV.

Mn_3Ge single crystals were grown by the flux method. Manganese powder (99.9%), germanium powder (99.99%) and cadmium pieces were mixed in a molar ratio of Mn:Ge:Cd = 7:2:48 and placed in an alumina crucible. This was sealed in a quartz tube under vacuum and heated to 950°C in 5 hours. The temperature was maintained for 20 hours before being slowly reduced to 650°C at a rate of 2°C/h . The quartz tube was subsequently removed from the furnace to cool to room temperature before being centrifuged to separate the single crystals from the cadmium flux. The flux growth produced shiny metallic needles (see Fig. 2) with hexagonal cross-sections and dimensions of up to $2 \times 0.4 \times 0.4 \text{ mm}^3$ (length along

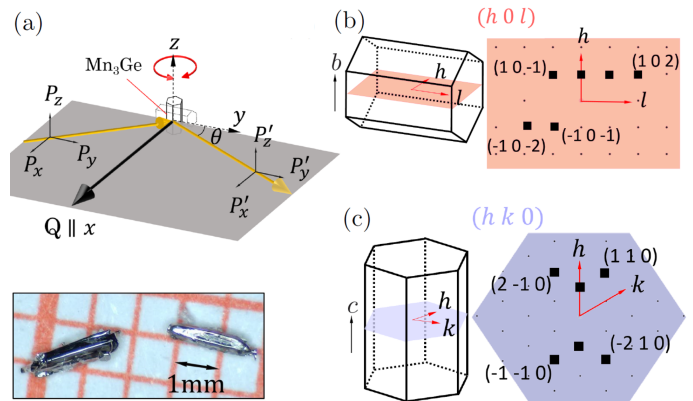


FIG. 2. (a) The experimental set-up of the SNP of Mn_3Ge in the horizontal diffraction geometry. The photograph shows flux-grown single crystals prepared in this work. (b) and (c) depict the crystal orientations with the b - and c -axis vertical, respectively, to access the $h0l$ and $hk0$ families of reflections. The reflections studied in this work are labeled with black squares.

the crystal c -axis). Single crystal x-ray diffraction patterns obtained from the crystals are consistent with the $P6_3/mmc$ space group and demonstrate that the crystals are of good crystalline quality, and the magnetic behaviour is consistent with previous data on Mn_3Ge (see Supplemental Material [22]).

SNP measurements were performed with the CRY-OPAD device installed on the D3 diffractometer at the Institut Laue-Langevin (Grenoble, France), with the sample contained in a zero-field chamber [31]. The technique involves determining the magnitude and direction of the polarization of the scattered neutrons when the incident neutrons are polarized along each of the principal directions x , y and z , where x is along the scattering vector \mathbf{Q} , z is perpendicular to the scattering plane, and y is chosen to complete the right-handed Cartesian set [see Fig. 2(a)]. The polarization of the scattered neutrons is resolved along the principal directions, giving a matrix \mathbf{P} whose elements P_{ij} represent the j component of the scattered polarization for an incident beam polarized in the i direction. A polarized, monochromatic incident beam was produced by diffraction from the (111) planes of a ferromagnetic crystal of Heusler alloy (Cu_2MnAl). Nutator and precession fields were used to control the direction of the incident polarization and the direction along which the scattered polarization was analysed. The scattered beam polarization was measured with a ^3He spin filter. A correction was made for the time decay of the efficiency of the filter based on measurements of a nuclear Bragg reflection with almost zero magnetic component.

The weak ferromagnetism of Mn_3Ge is a potential problem for SNP, as it could cause depolarization of the neutron beam in the sample. We adopted three strategies to alleviate this problem: (1) In the first set of measure-

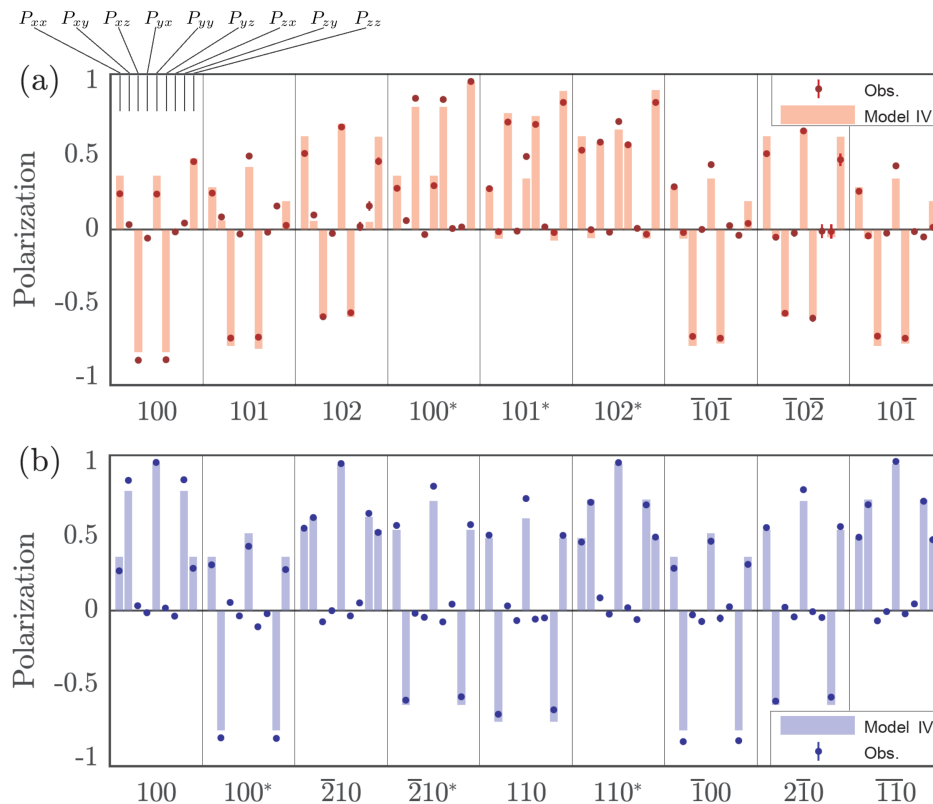


FIG. 3. Comparison between the observed and calculated polarization matrix elements P_{ij} for the Bragg peaks measured in the (a) ($h0l$), and (b) ($hk0$) scattering planes. For each reflection, the symbol and vertical bar represent (from left to right) P_{xx} , P_{xy} , P_{xz} , P_{yx} , P_{yy} , P_{yz} , P_{zx} , P_{zy} and P_{zz} , as indicated. Reflections marked with an asterisk (*) are measurements that were repeated with the incident polarisation reversed.

ments ($h0l$ reflections), the crystal was magnetized in a field of 1 T applied along the b -axis before it was installed in the cryostat mounted on CRYOPAD. This was done in order to reduce depolarization at the boundaries between magnetic domains [32]. (2) The dimensions of the crystal were relatively small, as mentioned earlier. (3) A relatively short neutron wavelength of $\lambda = 0.85 \text{ \AA}$ was used. Depolarization is proportional to the neutron wavelength and the integral of the magnetic flux along the neutron path through the sample. The field integral for a typical path length of 0.5 mm and remnant magnetization of $0.006 \mu_B/\text{Mn}$ is about $3 \times 10^{-6} \text{ Tm}$. This corresponds to a maximum neutron precession angle of about 7° at $\lambda = 0.85 \text{ \AA}$, which can be neglected.

The crystal of Mn_3Ge was first mounted with the b -

axis vertical, to access the $h0l$ reflections, and was subsequently remounted with the c -axis vertical in order to study the $hk0$ reflections [see Figs. 2(b) and (c)]. All measurements were made at a temperature $T = 2 \text{ K}$.

Figure 3 presents the set of measured polarization matrix elements P_{ij} for each of the reflections studied [see Figs. 2(b) and (c)]. Panels (a) and (b) contain data from the ($h0l$) and ($hk0$) scattering planes, respectively.

For a few reflections, indicated in Fig. 3 by an asterisk, measurements were made with the incident polarization reversed, as a check. We find that the neutrons suffer from negligible depolarization. This is best exemplified by the matrix elements P_{zz} for the 100^* reflection in Fig. 3(a) and P_{yy} for the 100 , $\bar{2}10$, 110^* and $\bar{1}\bar{1}0$ reflections in Fig. 3(b), which are all almost unity.

Using the MAG2POL program [28], which is based on the Blume–Maleev equations [33, 34], we set up the four different magnetic structure models depicted in Fig. 1. Where applicable, magnetic domains were also incorporated in the spin configuration models. For instance, for models III and IV, the spin configurations allow for six orientation domains, related by $\pm 60^\circ$ rotation of all of the in-plane Mn spins about the c -axis (although only three matter because the scattering cross-section is invariant

TABLE I. The reduced χ^2 goodness-of-fit statistic for the refinements of models I–IV against the measured polarization matrices in the two scattering planes investigated.

	I	II	III	IV
($h0l$)	21173	118434	577	336
($hk0$)	9603	165.61	9560	87

under 180° rotation of all the spins).

For each model I–IV, we calculated the full set of nine matrix elements for each of the measured reflections, and refined the length of the Mn moment and the domain populations (where applicable) via a least-squares fit to the measured polarization matrices (see Supplemental Material [22]). The data from the ($h0l$) and ($hk0$) scattering planes were fitted separately. The SNP technique is generally not sensitive to the length of the moment, but when the magnetic propagation vector is $\mathbf{k} = \mathbf{0}$, as in Mn_3Ge , the length of the moment can be obtained from the nuclear–magnetic interference scattering [29].

The values of the reduced χ^2 goodness-of-fit statistic obtained from the different refined models are tabulated in Table I. The values are large because the number of data points is large and the experimental errors are small. Additionally, the errors include counting statistics but exclude any sources of systematic error.

We find that the measured polarization matrices are described best by model IV, which is better than any of the other models by a significant margin. A comparison between the observed and calculated polarization matrices for model IV is given in Fig. 3. The agreement is seen to be very good, with deviations of only a few percent for the majority reflections. We also note that model IV is compatible with the observation of weak in-plane ferromagnetism, because only models III and IV allow a weak in-plane ferromagnetic moment while retaining the symmetry of the magnetic structure (see below).

The estimated moment length is $2.65(2)\mu_{\text{B}}$, which is in agreement with earlier studies [35, 36]. Moreover, the domain populations that give the best fit to the data are 60%, 36(3)% and 4(1)%, respectively. The significantly larger population of one domain over the other two in-plane orientations of Mn spins is consistent with the sample having been cooled from room temperature in a 1 T in-plane field.

There have been a number of attempts to determine the magnetic ground state of Mn_3Ge by *ab initio* density functional theory (DFT), with differing results [2, 10–14, 36]. References 2, 12–14, and 36 predict that the most stable spin configuration is model IV, consistent with our findings. On the other hand, Ref. 10 found the most stable magnetic structure to be model III, and Ref. 11 suggests that the Mn moments display non-planar order [11]. The difference in energy between models III and IV, which are related by an in-plane rotation of the Mn moments by 90°, is reported to be only a few meV, and at the limit of computational uncertainty of DFT [2, 10, 11, 13]. Moreover, owing to strong electronic correlations among the Mn 3d states, the electronic bands near the Fermi level are highly broadened, as also found in Mn_3Sn [37], making it difficult to ascertain which calculation best describes the band structure through comparison with angle-resolved photoemission spectroscopy. These problems emphasize that, as far as magnetic struc-

ture determination is concerned, *ab initio* studies are no substitute for experiment.

In order to understand certain aspects of the magnetic behavior we consider the effective spin Hamiltonian [15, 24, 25, 38–40],

$$\mathcal{H} = \mathcal{H}_{\text{H}} + \mathcal{H}_{\text{DM}} + \mathcal{H}_{\text{anis}}, \quad (1)$$

where \mathcal{H}_{H} describes nearest-neighbor Heisenberg exchange, \mathcal{H}_{DM} is the in-plane Dzyaloshinskii–Moriya (DM) interaction, and $\mathcal{H}_{\text{anis}}$ is the orthorhombic single-ion anisotropy. We make the assumptions (based on experiment) that the spins lie in the plane and that spins in one layer in the unit cell are parallel to those in inversion-related sites in the adjacent layer (see Fig. 1). The dependence of the Hamiltonian on the active degrees of freedom is then conveniently expressed in terms of four symmetry-adapted order parameters S , S' , \mathbf{A} and \mathbf{M} , which transform according to irreducible representations (irreps) of the point group D_{6h} (See Fig. 1 and Supplemental Material [22]). The first two transform as scalars under rotations, and have B_{1g} and B_{2g} symmetry, respectively. $\mathbf{M} = (M_x, M_y)$, which describes the average in-plane magnetization, and $\mathbf{A} = (A_x, A_y)$ are 2D irreps with E_{1g} symmetry. Spin structures III and IV shown in Fig. 1 correspond to modes A_x and A_y , respectively.

Explicit expressions for the order parameters are given in the Supplemental Material [22], and the Hamiltonian can be expressed in terms of these as

$$\begin{aligned} \mathcal{H} = & -\frac{J_1}{6}(S^2 + S'^2 + \mathbf{A}^2 - 2\mathbf{M}^2) \\ & + \frac{D}{2\sqrt{3}}(-S^2 - S'^2 + \mathbf{A}^2) \\ & + \frac{1}{3}\left\{K_1 S^2 + K_2 S'^2 + \frac{K_1 + K_2}{2}(\mathbf{A}^2 + \mathbf{M}^2) \right. \\ & \left. + (K_1 - K_2)\mathbf{A} \cdot \mathbf{M}\right\}. \end{aligned} \quad (2)$$

Here, J_1 is the nearest-neighbor in-plane exchange interaction, D is the DM interaction, and K_1 and K_2 are anisotropy constants perpendicular and parallel to the local easy axis, respectively.

The observed spin structure (Model IV) belongs to the \mathbf{A} order parameter, so assuming the hierarchy of interactions $|J_1| \gg |D| \gg K_{1,2}$ (Ref. 15) we can conclude that $J_1 > 0$ and $D < 0$. Moreover, once \mathbf{A} condenses, a small in-plane magnetization becomes inevitable through the coupling term $\mathbf{A} \cdot \mathbf{M}$. The weak ferromagnetism observed in Mn_3Ge arises, therefore, because the ground state magnetic structure has the same symmetry as \mathbf{M} .

The magnetic ground states described by \mathbf{A} form a one-parameter manifold $\mathbf{A} = A(\cos\theta, \sin\theta)$. The Hamiltonian (1)–(2) does not favour any particular θ , and hence does not account for why the system selects A_y ($\theta = \pi/2$) as its ground state. Indeed, earlier studies of the spin Hamiltonian of Mn_3Ge reported that the inverse triangular spin structure should have no in-plane

anisotropy energy up to fourth order [1, 15, 24, 25]. Anisotropy can be introduced if we include a sixth order term in Hamiltonian,

$$\begin{aligned}\mathcal{H}_6 &= C_1(A_x^3 - A_x A_y^2)^2 + C_2(A_y^3 - A_y A_x^2)^2 \\ &= \frac{A^6}{2} \{ (C_1 + C_2) + (C_1 - C_2) \cos 6\theta \}. \quad (3)\end{aligned}$$

This term, which has hexagonal anisotropy, splits the degeneracy of the ground state manifold of \mathbf{A} into two states, A_x and A_y (see Supplemental Material [22]). Given that the observed ground state magnetic structure is A_y , with $\theta = \pi/2$, we expect $C_1 - C_2 > 0$.

In conclusion, we have determined the magnetic structure of Mn_3Ge uniquely, and we have demonstrated that the weak in-plane ferromagnetism observed below T_N is intrinsic to Mn_3Ge and an inevitable consequence of the symmetry of the magnetic structure. We have also shown that the magnetic ground state is selected by sixth-order anisotropy. The results of this work will be important in future theoretical studies which address the discrepancies between the calculated and measured AHE in Mn_3Ge [1, 2, 11, 13, 16].

Neutron diffraction data from this study are available at Ref. [41].

Note added. During review of our manuscript, we became aware of a conventional polarized neutron diffraction study of Mn_3Ge which found the same magnetic structure as presented here [42].

The authors wish to thank S. Vial (ILL), D. Prabhakaran (Oxford) and M. C. Giordano (EPFL) for technical help, and N. Schröter (PSI) for interesting discussions. This work was supported by the U.K. Engineering and Physical Sciences Research Council (Grant Nos. EP/N034872/1 and EP/M020517/1), the Natural Science Foundation of Shanghai (Grant No. 17ZR1443300) and the National Natural Science Foundation of China (Grant No. 11874264). J.-R. Soh acknowledges support from the Singapore National Science Scholarship, Agency for Science Technology and Research.

* andrew.boothroyd@physics.ox.ac.uk

- [1] N. Kiyohara, T. Tomita, and S. Nakatsuji, Phys. Rev. Applied **5**, 064009 (2016).
- [2] A. K. Nayak, J. E. Fischer, Y. Sun, B. Yan, J. Karel, A. C. Komarek, C. Shekhar, N. Kumar, W. Schnelle, J. Kübler, C. Felser, and S. S. P. Parkin, Sci. Adv. **2**, e1501870 (2016).
- [3] N. Nagaosa, J. Sinova, S. Onoda, A. H. MacDonald, and N. P. Ong, Rev. Mod. Phys. **82**, 1539 (2010).
- [4] J. Balluff, J.-M. Schmalhorst, E. Arenholz, M. Meinert, and G. Reiss, Phys. Rev. B **97**, 014403 (2018).
- [5] H. Kurt, N. Baadji, K. Rode, M. Venkatesan, P. Stamenov, S. Sanvito, and J. M. D. Coey, Appl. Phys. Lett. **101**, 132410 (2012).
- [6] D. D. Dung, W. Feng, Y. Shin, and S. Cho, J. Appl. Phys. **109**, 07C310 (2011).
- [7] A. Sugihara, K. Suzuki, T. Miyazaki, and S. Mizukami, Metals **5**, 910 (2015).
- [8] T. Ogasawara, J. young Kim, Y. Ando, and A. Hirohata, J. Magn. Magn. Mater. **473**, 7 (2019).
- [9] J. Jeong, Y. Ferrante, S. V. Faleev, M. G. Samant, C. Felser, and S. S. P. Parkin, Nat. Comms. **7**, 10276 (2016).
- [10] G.-Y. Guo and T.-C. Wang, Phys. Rev. B **96**, 224415 (2017).
- [11] J. Kübler and C. Felser, Europhys. Lett. **108**, 67001 (2014).
- [12] Y. Zhang, Y. Sun, H. Yang, J. Železný, S. P. P. Parkin, C. Felser, and B. Yan, Phys. Rev. B **95**, 075128 (2017).
- [13] J. Kübler and C. Felser, Europhys. Lett. **120**, 47002 (2017).
- [14] H. Yang, Y. Sun, Y. Zhang, W.-J. Shi, S. S. P. Parkin, and B. Yan, New J. Phys. **19**, 015008 (2017).
- [15] J. Liu and L. Balents, Phys. Rev. Lett. **119**, 087202 (2017).
- [16] N. Ito and K. Nomura, J. Phys. Soc. Jpn. **86**, 063703 (2017).
- [17] Y. Zhang, J. Železný, Y. Sun, J. van den Brink, and B. Yan, N. J. Phys. **20**, 073028 (2018).
- [18] B. Nyári, A. Deák, and L. Szunyogh, Phys. Rev. B **100**, 144412 (2019).
- [19] H. Chen, Q. Niu, and A. H. MacDonald, Phys. Rev. Lett. **112**, 017205 (2014).
- [20] N. Yamada, H. Sakai, H. Mori, and T. Ohoyama, Physica B **149**, 311 (1988).
- [21] J. S. Kouvel and J. S. Kasper, Proc. Conf. on Magn. , 169 (1965).
- [22] See Supplemental Material at <http://link.aps.org/supplemental/...> for single crystal x-ray diffraction data, magnetometry measurements, neutron scattering data and symmetry analysis.
- [23] G. Kádár and E. Krén, Int. J. Magn. **1**, 143 (1971).
- [24] S. Tomiyoshi, Y. Yamaguchi, and T. Nagamiya, J. Magn. Magn. Mater. **31-34**, 629 (1983).
- [25] T. Nagamiya, S. Tomiyoshi, and Y. Yamaguchi, Solid State Commun. **42**, 385 (1982).
- [26] P. J. Brown, T. Chattopadhyay, J. B. Forsyth, and V. Nunez, J. Phys.: Condens. Matter **3**, 4281 (1991).
- [27] P. J. Brown, Physica B: Condensed Matter **297**, 198 (2001).
- [28] N. Qureshi, J. Appl. Cryst. **52**, 175 (2019).
- [29] T. Chatterji, ed., Neutron Scattering from Magnetic Materials (Elsevier, 2006) Chap. 5.
- [30] P. J. Brown, V. Nunez, F. Tasset, J. B. Forsyth, and P. Radhakrishna, J. Phys.: Condens. Matter **2**, 9409 (1990).
- [31] E. Lelièvre-Berna, E. Bourgeat-Lami, P. Fouilloux, B. Geffray, Y. Gibert, K. Kakurai, N. Kernavanois, B. Longuet, F. Mantegazza, M. Nakamura, S. Pujol, L.-P. Regnault, F. Tasset, M. Takeda, M. Thomas, and X. Tonon, Physica B: Condensed Matter **356**, 131 (2005).
- [32] In retrospect, this procedure was probably not effective, because for the second set of measurements ($hk0$ reflections) we did not pre-magnetize the sample, and in neither case did we find any evidence for depolarization.
- [33] M. Blume, Phys. Rev. **130**, 1670 (1963).
- [34] S. V. Maleev, V. G. Bar'yakhtar, and R. A. Suris, Sov.

- Phys. Solid State **4**, 2533 (1963).
- [35] A. S. Sukhanov, S. Singh, L. Caron, T. Hansen, A. Hoser, V. Kumar, H. Borrmann, A. Fitch, P. Devi, K. Manna, C. Felser, and D. S. Inosov, Phys. Rev. B **97**, 214402 (2018).
 - [36] D. Zhang, B. Yan, S.-C. Wu, J. Kübler, G. Kreiner, S. S. P. Parkin, and C. Felser, J. Phys.:Condens. Matter **25**, 206006 (2013).
 - [37] K. Kuroda, T. Tomita, M.-T. Suzuki, C. Bareille, A. A. Nugroho, P. Goswami, M. Ochi, M. Ikhlas, M. Nakayama, S. Akebi, R. Noguchi, R. Ishii, N. Inami, K. Ono, H. Kumigashira, A. Varykhalov, T. Muro, T. Koretsune, R. Arita, S. Shin, T. Kondo, and S. Nakatsuji, Nat. Mater. **16**, 1090 (2017).
 - [38] J. Sticht, K.-H. Höck, and J. Kübler, J. Phys.: Condens. Matter **1**, 8155 (1989).
 - [39] T. Nagamiya, J. Phys. Soc. Jpn. **46**, 787 (1979).
 - [40] G. J. Zimmer and E. Krén, AIP Conf. Proc. **10**, 1379 (1973).
 - [41] A. T. Boothroyd, H. Jacobsen, N. Qureshi, and J.-R. Soh, (2018), 10.5291/ILL-DATA.5-41-975.
 - [42] Y. Chen, J. Gaudet, S. Dasgupta, G. G. Marcus, J. Lin, T. Chen, T. Tomita, M. Ikhlas, Y. Zhao, W. C. Chen, M. B. Stone, O. Tchernyshyov, S. Nakatsuji, and C. Broholm, arXiv: 2001.09495 (2020).